ChemPubSoc Europe

DOI: 10.1002/chem.201504867

CHEMISTRY A European Journal Full Paper

Porous Materials | *Very Important Paper* |

VIP Metal–Organic Framework-Templated Porous Carbon for Highly Efficient Catalysis: The Critical Role of Pyrrolic Nitrogen Species

Gang Huang[+], Li Yang[+], Xiao Ma, Jun Jiang,* Shu-Hong Yu, and Hai-Long Jiang*[a]

Abstract: Metal-free catalysts are of great importance and alternative candidates to conventional metal-based catalysts for many reactions. Herein, several types of metal–organic frameworks have been exploited as templates/precursors to afford porous carbon materials with various nitrogen dopant forms and contents, degrees of graphitization, porosities, and surface areas. Amongst these materials, the PCN-224-templated porous carbon material optimized by pyrolysis at 700 °C (denoted as PCN-224-700) is composed of amorphous carbon coated with well-defined graphene layers, offering a high surface area, hierarchical pores, and high nitrogen content (mainly, pyrrolic nitrogen species). Remarkably, as a metal-free catalyst, PCN-224-700 exhibits a low activation energy and superior activity to most metallic catalysts in the catalytic reduction of 4-nitrophenol to 4-aminophenol. Theoretical investigations suggest that the content and type of the nitrogen dopant play crucial roles in determining the catalytic performance and that the pyrrolic nitrogen species makes the dominant contribution to this activity, which explains the excellent efficiency of the PCN-224-700 catalyst well.

Introduction

Catalysis is an important and widely investigated subject both in fundamental and industrial chemistry. The heart of catalytic chemistry is centered on the design of catalysts, in which metal, metal oxide, metal complexes, and so forth are undoubtedly the most vibrant for many paramount reactions in modern chemistry. However, metal catalysts with limited reserves are normally expensive and often not stable enough. To achieve green and sustainable chemistry, it is highly desirable to develop metal-free catalysts. Carbon materials, as one class of important metal-free catalyst, have recently sparked intense interest and been extensively studied in many reactions, such as the oxygen reduction reaction (ORR) in fuel cells and the oxidation and reduction reactions with various substrates.[1] Carbon materials, which possess different dimensionalities (0 to 3D) and mainly include fullerene and its derivatives, carbon nanotubes, graphene (oxides), and porous carbon, are cheap, stable, recyclable, biocompatible, environmentally friendly, and readily available. Porous carbon materials in 3D structures afford highly developed internal surface areas and large porosities, which facilitate the adsorption and concentration of catalytic substrates, minimize diffusion limitations, and catalyst deactivation, thus greatly meriting the conversion.

On the other hand, the surface chemistry of the carbon material plays a decisive role in its catalysis by offering active sites that can chemisorb the reactants and provide surface intermediates of sufficient strength. Doping with hetero atoms into carbon materials has been demonstrated to be an effective method to manipulate the surface chemistry, tailor the electronic properties, and make local changes to the elemental composition, thus improving the catalytic performance.[2] Among the diverse potential dopants in carbon materials, nitrogen atoms are considered to be an excellent choice due to their comparable atomic size and five valence electrons, which is beneficial for the formation of strong valence bonds with carbon atoms. Many routes, such as electrical-joule heating in an ammonia atmosphere, thermal treatment in an ammonia atmosphere, hydrothermal reaction with urea, and so forth, have been developed to dope nitrogen atoms into various carbon materials.[3] Depending on the synthetic techniques, an inhomogeneous distribution of nitrogen dopants and a subsurface region of nitrogen doping at a very limited depth are common, whereas the highly uniform nitrogen doping throughout the whole materials remains a significant challenge.

To obtain porous carbon materials with a homogeneous distribution of nitrogen atoms, metal–organic frameworks (MOFs)[4] could be ideal templates and precursors. As a class of crystalline porous material, MOFs consisting of metal ions/clusters and rigid organic linkers have been demonstrated to be functional materials for a wide variety of applications.[5–8] Re-

[a] *G. Huang,[+] L. Yang,[+] X. Ma, Prof. Dr. J. Jiang, Prof. Dr. S.-H. Yu, Prof. Dr. H.-L. Jiang*
Hefei National Laboratory for Physical Sciences at the Microscale
CAS Key Laboratory of Soft Matter Chemistry
Collaborative Innovation Center of Suzhou Nano Science and Technology
School of Chemistry and Materials Science
University of Science and Technology of China
Hefei, Anhui 230026 (P.R. China)
E-mail: jianglab@ustc.edu.cn
jiangj1@ustc.edu.cn

[+] *These authors contributed equally to this work.*

Supporting information and ORCID(s) from the author(s) for this article are available on the WWW under http://dx.doi.org/10.1002/chem.201504867.

cently, MOFs have been exploited to prepare porous carbon materials with exceptionally high specific surface areas by means of pyrolysis at high temperature in an inert atmosphere,[9,10] and the MOF-derived porous carbon materials have been applied to energy-related applications, such as in supercapacitors, the oxygen reduction reaction (ORR), lithium-ion batteries, and so forth.[9,10] The periodic arrangement of different atoms in highly ordered MOFs as precursors/templates offers congenital conditions for homogeneous atomic distribution. Therefore, MOFs based on nitrogen-containing organic ligands would enable the resultant nitrogen atoms to be well distributed throughout the porous carbon matrix upon pyrolysis. In addition, the resultant nitrogen percentages are readily tunable by controlling the nitrogen content of the ligands/MOFs or the subsequent pyrolysis temperatures.

Bearing this approach in mind, three representative MOFs (i.e., MOF-5 without nitrogen atoms, ZIF-8, and PCN-224 containing different types of nitrogen species)[11] were selected as hard templates and precursors to afford porous carbon materials, namely, MOF-5-*T*, ZIF-8-*T*, and PCN-224-*T* (*T* = pyrolysis temperature), upon pyrolysis. The content and form of the nitrogen dopant involved in the resultant porous carbon materials and their surface areas are dependent on the MOF templates and pyrolysis temperatures. The porous carbon material obtained by pyrolysis of PCN-224 at 700 °C exhibits excellent catalytic performances and an even lower apparent activation energy than most metallic catalysts in the hydrogenation of 4-nitrophenol (4-NP). To elucidate the mechanism behind the high catalytic efficiency of PCN-224-700, first-principles simulations at the density functional theory (DFT) level were performed. The charge polarization effect, molecule adsorption, and electron migration abilities of three model structures of nitrogen-doped graphene (NG) were examined. It is revealed that the accumulation of a high positive charge density by the pyrrolic nitrogen structure in PCN-224-700 results in a strong metal-like property, which greatly enhances the catalytic ability. This result is in good agreement with the highest pyrrolic nitrogen content and best catalytic activity of PCN-224-700 of all the investigated porous carbon-based catalysts.

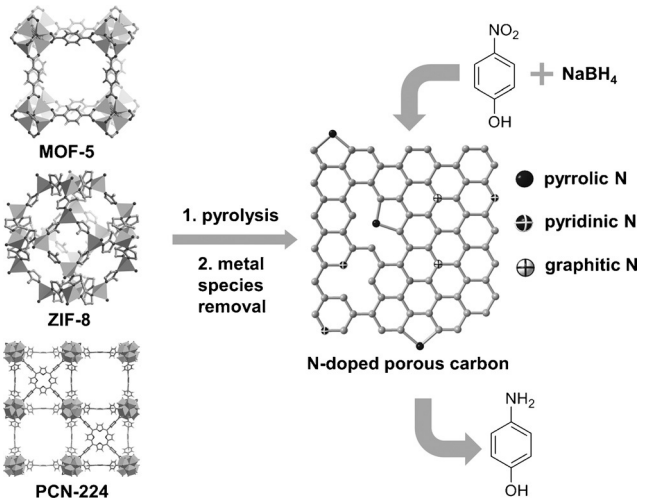

Scheme 1. Schematic illustration for the synthesis of nitrogen-doped porous carbon materials by the pyrolysis of different MOFs.

Results and Discussion

Synthesis and characterization

The three representative MOFs, that is, MOF-5, ZIF-8, and PCN-224, were prepared based on previous reports,[11] and their purity was shown by using powder X-ray diffraction (PXRD; see Figure S1 in the Supporting Information). The MOFs underwent pyrolysis at different temperatures in a N_2 atmosphere, followed by acid etching and washing to remove the residual metal (oxide) to give porous carbon materials (Scheme 1), which are denoted as MOF-5-*T*, ZIF-8-*T*, and PCN-224-*T*, respectively.

The PXRD patterns for the MOF-templated carbon materials exhibit two peaks at around 25 and 44° indexed to the characteristic (002) and (101) diffraction patterns of carbon (see Figure S2 in the Supporting Information). The considerable (002) peak in the ZIF-8- and PCN-224-templated samples shifts toward a comparatively sharp peak at 26°, in stark contrast to the broad peak at approximately 23° of the MOF-5-templated carbon matrix. This outome suggests an improved degree of graphitization in the former carbon materials. The result is further supported by Raman spectroscopic analysis. The degree of graphitization of carbon (*R*) can be evaluated by the ratio of integrated intensity of the D and G bands ($\tilde{\nu} = 1360$ and 1580 cm^{-1}, respectively; $R = I_D/I_G$) As expected, PCN-224-700 has the lowest *R* value, which indicates a higher degree of graphitization relative to the other carbon materials (Figure 1a).[12] Nitrogen sorption experiments were performed to examine the pore textures and surface areas of the MOF-derived porous carbon materials at different pyrolysis temperatures (see Figure 1b–d and Table S1 in the Supporting Information). Amongst these materials, MOF-5-1000 has the highest BET surface area of 2084 m^2g^{-1}. The BET surface areas of ZIF-8-1000 and PCN-224-700 are 1289 and 1089 m^2g^{-1}, respectively, thus representing the highest values among their respective MOF-derived carbon materials. In addition, pore size distribution analysis indicates that the carbon materials derived from ZIF-8 are almost microporous, whereas both MOF-5- and PCN-224-templated carbon materials generally possess hierarchical pores (see Figure S3 in the Supporting Information), which, in addition to the large surface area and pore volume, would be beneficial because of the exposure of active sites and rapid transportation of the catalytic substrates/products.

Scanning electron microscopy (SEM) for the pyrolysis products MOF-5-1000, ZIF-8-1000, and PCN-224-700 shows that the morphology of the original MOFs can be mostly retained, although the sizes shrink to some extent after pyrolysis (see Figure S4 in the Supporting Information). Given the absence of nitrogen atoms in pristine MOF-5, the pyrolysis product should be based on carbon only. In comparison, elemental analysis shows that the nitrogen contents of ZIF-8-1000 and PCN-224-700 are 4.41 and 3.08 wt%, respectively, in agreement with the high nitrogen contents of their parent MOFs (the theoretical

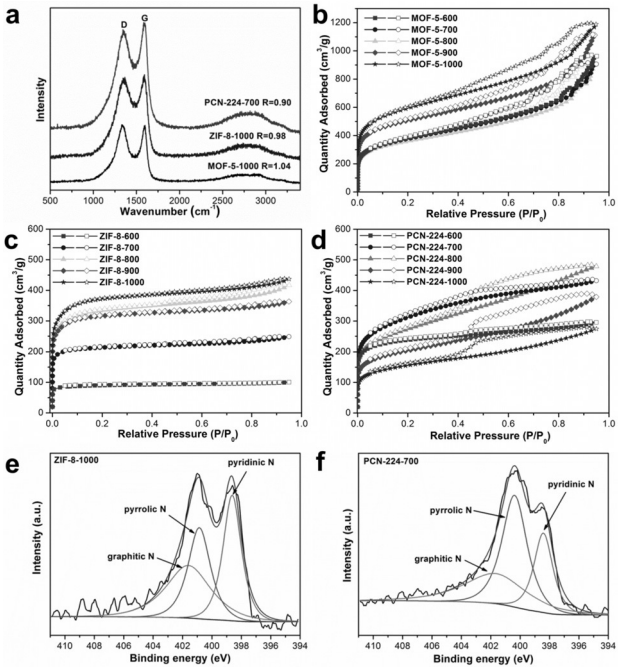

Figure 1. a) Raman spectra of MOF-5-1000, ZIF-8-1000, and PCN-224-700. Nitrogen adsorption and desorption isotherms for b) MOF-5-*T*, c) ZIF-8-*T*, and d) PCN-224-*T* ($T=600$, 700, 800, 900, and 1000 °C). The high-resolution N 1s XPS spectra for e) ZIF-8-1000 and f) PCN-224-700.

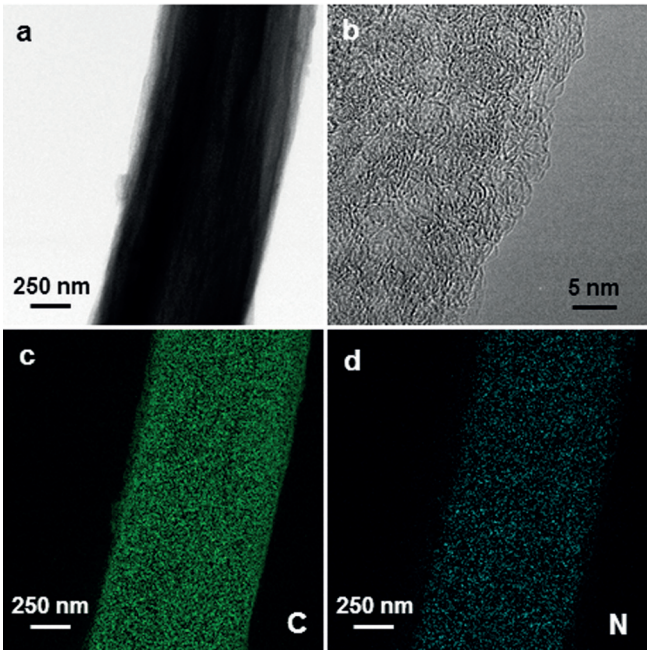

Figure 2. The a) TEM and b) HRTEM images of PCN-224-700. c, d) Elemental mapping images of the carbon and nitrogen atoms, respectively, in PCN-224-700.

nitrogen contents of ZIF-8 and PCN-224 are 24.40 and 4.10 wt%, respectively). High-resolution X-ray photoelectron spectroscopy (XPS) for N 1s in ZIF-8-1000 and PCN-224-700 showed that there are three types of nitrogen species: pyridinic, pyrrolic, and graphitic nitrogen (see Figure 1e,f and Table S2 in the Supporting Information). Notably, the ratio of diverse types of N species is different in these materials; that is, the percentage of pyrrolic nitrogen atoms in ZIF-8-1000 is much lower than in PCN-224-700 (30.48 vs. 45.45%, respectively) possibly due to the fact that PCN-224 has a high pyrrole content. In addition, no high-contrast particles can be observed in the transmission electron microscopy (TEM) image (see Figure S5 in the Supporting Information), thus revealing the complete removal of metal (oxide) species upon acid etching, which is in accordance with the results of the PXRD and thermogravimetric (TG) analysis (see Figures S2 and S6, respectively, in the Supporting Information). High-resolution TEM images of PCN-224-700 clearly present an amorphous carbon structure coated by well-defined graphene layers on the edge of the rodlike structure (Figure 2b). The amorphous internal carbon atoms are in agreement with the fair intensity of the (002) peak in the PXRD pattern mentioned above, whereas the graphene layer coatings could be crucial to the catalytic behavior. Elemental mapping indicates that PCN-224-700 is mainly composed of carbon and nitrogen species (Figure 2c,d), in which nitrogen atoms are dispersed uniformly throughout the carbon matrix, thus demonstrating the niche of the MOF precursor.

Catalytic activity evaluation

The above results demonstrate the well-defined porous structure, high surface area, and homogeneous nitrogen doping for the MOF-templated carbon materials, which thus encouraged us to investigate the catalytic reduction of 4-nitrophenol (4-NP; one of the most universal organic pollutants in waste waters from agricultural and industrial sources) to 4-aminophenol (4-AP) by $NaBH_4$ in water under ambient conditions. The reaction progress was observed by the naked eye (see Figure S7 in the Supporting Information), and the reduction kinetics were recorded by using UV/Vis absorption spectroscopic analysis, which showed a decreasing characteristic peak at $\lambda=$ 400 nm for the 4-NP ion and an increasing characteristic peak at $\lambda=300$ nm for the 4-AP ion. The conversion from a nitro into an amino compound has great industrial value, and this reduction reaction represents an important probe of the catalytic activity, which usually uses metallic catalysts.[13] However, very few metal-free catalysts are highly active for this reaction.[14]

It is well known that the reaction does not proceed in the absence of a catalyst. Upon the introduction of the MOF-templated catalyst, the reaction proceeds effectively. The MOF-5-*T* ($T\leq 700$ °C) matrix has negligible activity, possibly due to the relatively low surface area, low degree of graphitization, and lack of nitrogen dopant in the catalyst. At higher pyrolysis temperatures, the product can catalyze the conversion of 4-NP and the catalytic activity increases with the pyrolysis temperature (see Figure S8a in the Supporting Information), which could be explained by the larger surface area, pore volume, and improved degree of graphitization in the catalyst obtained at higher temperatures. Similar to MOF-5-*T*, ZIF-8-*T* with a pyrolysis

temperature lower than 700 °C is almost inactive. Although the resultant carbon materials ZIF-8-*T* show evident activity upon pyrolysis at elevated temperatures, the reaction kinetics are even significantly lower than for MOF-5-*T* prepared at the same temperature (see Figure S8b in the Supporting Information). This result can be attributed to the only microporosity that exists in ZIF-8-*T*, which is detrimental to the transportation of the catalytic substrate/product, thus slowing the catalytic reaction kinetics. Unexpectedly and in contrast to the previous two examples, the pyrolysis product of PCN-224 exhibits considerable activity, even at 600 °C, and PCN-224-700 possesses the best activity among all the obtained carbon materials, possibly due to the high pyrrolic nitrogen content, hierarchical porosity, and good degree of graphitization (see Figure S8c in the Supporting Information), as described above. The activities of the PCN-224-templated products gradually decreases with the pyrolysis temperatures, which could be dominated by the surface area.

Among the different MOF-templated carbon materials, it is clear that PCN-224-700 has a much higher activity than MOF-5-1000 and ZIF-8-1000 (Figure 3a). As expected, the reaction over PCN-224-700 presents pseudo-first-order kinetics and the reaction rate constant is up to $k = 5.3 \times 10^{-3}\,s^{-1}$, which, to the best of our knowledge, is higher than all the reported metal-free catalysts[14] and even superior to many metallic catalysts.[15] Given that the PCN-224-700 catalyst is prepared at high temperatures, it is very stable and thus can be readily recycled and reused. The three reaction runs displayed in Figure 3b show almost the same catalytic activity curves, thus demonstrating the perfect stability and recyclability of PCN-224-700. To calculate the apparent activation energy (E_a), the reaction rate constant of the PCN-224-700 obtained in the range of 274–298 K was calculated to be 26.4 kJ mol^{-1} (Figure 3b inset), which is lower than most of previously reported metallic catalysts.[15c,d,16] With such a low activation energy, PCN-224-700 gives an even better performance than most metallic catalysts.

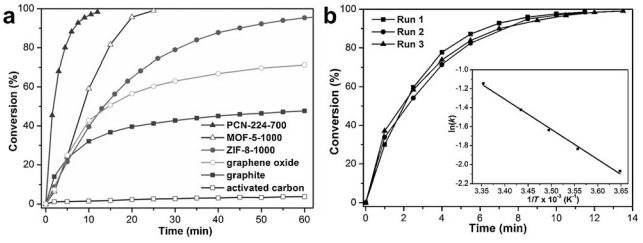

Figure 3. a) Catalytic conversion of 4-NP over activated carbon, graphite, graphene oxide, MOF-5-1000, ZIF-8-1000, and PCN-224-700. b) The catalytic conversion of 4-NP for three cycles over PCN-224-700 (inset: Arrhenius plots of the rate constant of the reduction of 4-NP by PCN-224-700).

It is generally accepted that catalytic activity connected to the structure of carbon-based porous catalysts is influenced by the following factors: 1) high surface area of the catalyst, thus enabling the active sites to be more accessible; 2) porosity and pore sizes, as large pores merit the transportation of catalytic substrates/products; 3) degree of graphitization of the carbon catalyst; and 4) the heteroatom involved in the structure.[17] To understand the effect of the degree of graphitization further, the activities of commercial graphite and activated carbon materials were investigated in the catalytic reduction of 4-NP to 4-AP. The activated carbon material in the amorphous state is almost inactive, although its surface area is very high (1396 m^{2}g^{-1}), whereas the nonporous graphite material shows a fair catalytic behavior (see Figure 3a and Figure S9 in the Supporting Information), possibly due to the delocalized bonds that exist in the graphitized catalyst. For comparison, graphene oxide (GO) was also investigated with respect to the catalytic reaction, and its activity was higher than graphite but lower than all the MOF-templated carbon materials (Figure 3a). In addition, the heteroatom dopant, namely, the nitrogen atom, can change the electron cloud density of the delocalized bond and thus improve the catalytic activity.

In fact, these factors would synergistically affect the activity of a given catalyst. For example, MOF-5-1000 possesses an even better activity than ZIF-8-1000; although the former material does not contain the nitrogen heteroatom as catalytic active site, it has a higher surface area and pore volume and contains hierarchical pores. The much higher activity of PCN-224-700 relative to MOF-5-1000 could be mainly ascribed to the absence of the nitrogen atom active sites in the latter catalyst. However, the mechanism behind the lower activity of ZIF-8-1000 relative to PCN-224-700 becomes rTHER complicated because the degrees of graphitization and nitrogen contents of these materials are similar, whereas the surface area of the former is even higher. Given the significantly different forms of nitrogen in these two catalysts, we assume that the nature of the nitrogen species involved in the structure plays a critical role in the activity.

Theoretical investigation

To elucidate the mechanism further behind the high catalytic efficiency of PCN-224-700, especially the influence of the nitrogen form, nitrogen-doped graphene (NG) models were built to investigate their structural and electronic properties before and after interaction with the 4-NP molecule. Geometry optimization calculations give three stable NG structures, which consist of separate pyrrolic, pyridinic, and graphitic rings (Figure 4a). The adsorption of a 4-NP$^-$ molecular ion on those three NG systems through the hydroxy and nitro groups[14b] were simulated, with the optimized NG@4-NP$^-$ structures displayed in Figure 4b,c, respectively. The pyrrolic NG system involves the bonding of a nitrogen atom to two carbon atoms (C1 and C2) and one hydrogen atom (H), the pyridinic NG system has only two N–C bonds (C1 and C2), and the graphitic NG system contains three N–C bonds (C1, C2, and C3).

Normally, carbon atoms in graphene hold negative or neutral charges. However, when an nitrogen atom is doped, the *ortho*-carbon and *ortho*-hydrogen atoms around that nitrogen atom could accumulate positive charges.[18] Thus, we examined the charge distribution present. As expected, the nitrogen atoms tend to accumulate negative charges to result in positive charges on those atoms around the nitrogen atom

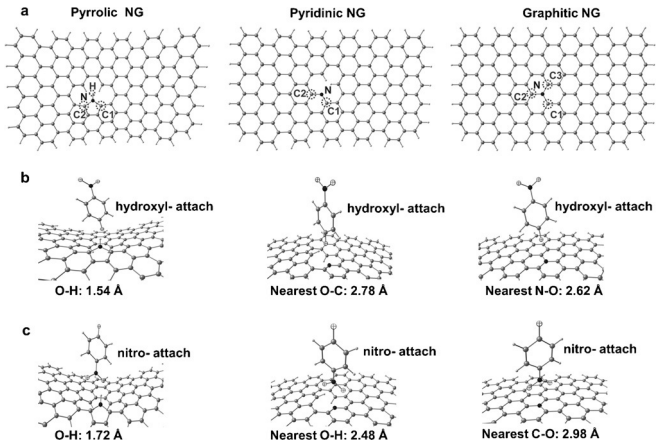

Figure 4. a) The optimized structures of pyrrolic NG, pyridinic NG, and graphitic NG systems. b, c) The adsorption structures of 4-NP$^-$ molecular ions on three NG systems through the hydroxy and nitro moieties, respectively. The black, middle gray, light gray, and crossed circles stand for the N, C, H, and O atoms, respectively.

Table 1. The charges of *ortho*-carbon, *ortho*-hydrogen, and nitrogen atoms of three NG systems.[a]

Pyrrolic NG	Charge [e]	Pyridinic NG	Charge [e]	Graphitic NG	Charge [e]
N	−0.56	N	−0.44	N	−0.31
C1	0.17	C1	0.22	C1	0.22
C2	0.17	C2	0.22	C2	0.21
H1	0.46	–	–	C3	0.23

[a] The positive electron number is the unit of the charge.

(Table 1). The strongest charge polarization occurs in the pyrrolic NG system, as reflected by the number of positive charges on the C1, C2, and H atoms. It is known that positive charges help to attract the terminal oxygen atoms (often negative charged) of the 4-NP$^-$ ion, thereby facilitating adsorption. This behavior explains the fact that the contact distance between the pyrrolic NG system with the 4-NP$^-$ ion is significantly smaller than the other two cases. Therefore, the pyrrolic NG structure, with the strongest positive polarization charges around the nitrogen atom, exhibits the biggest adsorption energies for the 4-NP$^-$ ion in the hydroxy- or nitro-attaching situations (Table 2). Consequently, strong coupling of electronic structures was found in the pyrrolic NG@4-NP$^-$ system. It can be seen that the NG part donates a positive charge of approximately 0.10–0.13 e to the 4-NP$^-$ ion (Table 2). This behavior

Table 2. The adsorption energies (E_{ad}) and charges being donated to the 4-NP$^-$ ion by the NG system (ΔCharge) in the three NG@4-NP$^-$ model systems, in which the molecules are attached to the NG structure through the hydroxy or nitro groups.

Structure	Hydroxy attachment		Nitro attachment	
	E_{ad} [eV]	ΔCharge [e]	E_{ad} [eV]	ΔCharge [e]
pyrrolic NG@4-NP$^-$	0.94	0.10	0.82	0.13
pyridinic NG@4-NP$^-$	0.27	0.06	0.30	0.18
graphitic NG@4-NP$^-$	0.73	0.03	0.73	0.09

inevitably promotes the activation of the 4-NP$^-$ ion because its reduction to the 4-AP form is driven by positive charges. Meanwhile, the pyridinic NG structure can donate more positive charges (0.18 e) to the 4-NP$^-$ molecular ion through the nitro-group adsorption (Table 2), whereas its adsorption energy is still much lower than the pyrrolic NG@4-NP$^-$ system.

One of the advantages of metallic catalysts is good electric conductivity, which helps to deliver energetic charge to trigger chemical reactions. It is well known that graphene has excellent electric conductivity,[19] and our NG systems might also maintain the ability to deliver charge to drive the reduction of the 4-NP$^-$ ion.[20] We display the calculated partial density of states (PDOS) for the different regions in the NG systems in Figure 5. We defined region **2** as the part that contains the

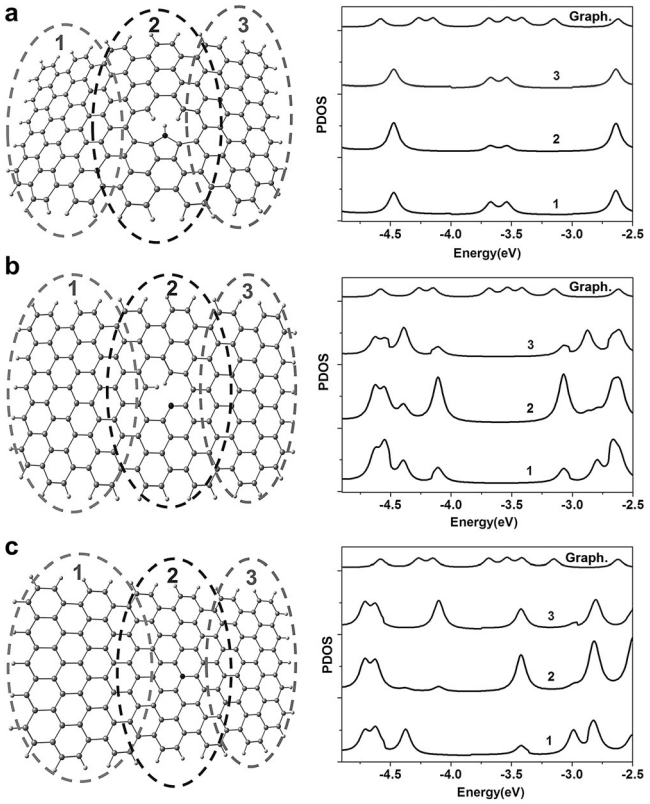

Figure 5. The computed partial density of states (PDOS) of different regions in the a) pyrrolic NG, b) pyridinic NG, and c) graphitic NG systems. Region **2** contains the doped nitrogen species, whereas regions **1** and **3** are the non-doped graphene parts aside region **2**.

doped nitrogen species, whereas regions **1** and **3** are non-doped with graphene parts aside region **2**. Obviously, the PDOS features of regions **1**–**3** in the pyrrolic NG system are similar to each other and are all close to that of pure graphene. This scenrio means that the pyrrolic NG system still maintain the same electron transportation ability as graphene, which is helpful in catalytic applications by efficiently delivering an abundant electron source. In contrast, the PDOS of regions **1** and **3** are very different to region **2** in the pyridinic and graphitic NG system, thus implying the breakdown of the

electron transportation channels from region **1** to **3**. Therefore, the pyrrolic NG structure achieves the advantages of metal catalysts without including metallic atoms by offering adsorption sites for further catalytic reactions and providing efficient channels to deliver energetic charge for these reactions. These results are consistent with previous reports that have shown that the doped nitrogen atoms could induce a local charge density and create metal-like properties.[14b]

Conclusion

Three different types of representative MOF materials, that is, MOF-5, ZIF-8, and PCN-224, have been exploited as hard templates to obtain metal-free porous carbon materials. The resultant carbon materials have exhibited high surface areas, microporous/hierarchically porous structures, and various degree of graphitizations; furthermore, these materials possess different types of nitrogen species in the frameworks, depending on the pyrolysis temperature and parent MOF structure. The experimental results have clearly shown that the MOF-templated carbon materials are very active toward the catalytic reduction of 4-NP to 4-AP in the presence of $NaBH_4$ under ambient conditions. The catalytic performance is highly dependent on the structural character of the resultant porous carbon catalysts. The PCN-224-700 matrix outperformed all the other counterparts and presents a great potential for industrial chemistry because of its excellent activity, stability, and recyclability. Theoretical investigations have suggested that the content and type of the nitrogen dopants are important for the catalytic conversion. Three types of nitrogen species, especially the pyrrolic nitrogen species, have shown a strong ability to absorb 4-NP ions, activate the nitro groups, and deliver energetic charges. Thus, is has been found that the pyrrolic nitrogen species makes the greatest contribution to the high catalytic performance, which is in consistent with the high pyrrolic nitrogen contents and excellent catalytic efficiency of the PCN-224-700 catalyst. These results shed light on the component and structure of doped carbon catalysts and the influence of these factors on the activity. This study can pave the way to rational design and the development of metal-free carbon materials for highly efficient catalysis.

Experimental Section

Materials and instrumentation

All chemicals were obtained from commercial sources and used without further purification. Tetrakis(4-carboxyphenyl)porphyrin (H_2TCPP) was prepared according to the procedures described in the Supporting Information. Distilled water with a specific resistance of 18.25 $M\Omega\,cm^{-1}$ was obtained by using reversed osmosis followed by ion-exchange and filtration (Cleaned Water Treatment Co., Ltd., Hefei, China). SEM was performed on a Zeiss Supra 40 apparatus at an acceleration voltage of 5 kV. TEM was performed on a Hitachi H-7650 transmission electron microscope at an acceleration voltage of 120 kV. High-resolution TEM and elemental mapping were performed on a JEOL-2100F transmission electron microscope at an acceleration voltage of 200 kV. PXRD patterns of the product were obtained on a Japan Rigaku DMax-γA rotation anode X-ray diffractometer equipped with graphite monochromatized CuKα radiation ($\lambda = 1.54$ Å). TG analysis was performed on a TGA Q5000 integration thermal analyzer at a heating rate of 10 °C in an air atmosphere. UV/Vis spectra of the samples were recorded on a UV/Vis spectrophotometer (TU-1810, Beijing Pgeneral, China). The nitrogen content was measured on a VarioELIII elemental analyzer. Raman-scattering spectra were recorded on a Renishaw System 2000 spectrometer by using Ar^+ for excitation ($\lambda =$ 514.5 nm). XPS measurements were performed on a Thermo ESCALAB 250 high-performance electron spectrometer by using monochromatized AlKα ($h\nu = 1486.7$ eV) as the excitation source. Nitrogen sorption measurements were conducted on a Micromeritics ASAP 2020 system at 77 K. Prior to the measurements, the carbon materials were activated at 120 °C in a dynamic vacuum for 24 h. Electrochemical experiments were performed on a CHI 760E electrochemical workstation in a 2 M solution of H_2SO_4. Before the measurements, the capacitor cell was evacuateded for 30 min in a 2 M H_2SO_4 electrolyte.

Preparation of MOFs

Synthesis of MOF-5: The synthesis of MOF-5 was based on a modified previous report.[11b] Typically, terephthalic acid (0.51 g) and triethylamine (0.85 mL) were dissolved in DMF (40 mL) and $Zn(OAc)_2{\cdot}2H_2O$ (1.7 g) was dissolved in DMF (50 mL). The two solutions were mixed and vigorously stirred for 2.5 h at room temperature. The resultant particles were collected by centrifugation and immersed in DMF overnight. The precipitate was separated and immersed in $CHCl_3$, which was exchanged twice in 2 days. The resultant product was collected by centrifugation and dried under vacuum overnight at room temperature.

Synthesis of ZIF-8: The synthesis of ZIF-8 was based on a modified previous report.[11e] Typically, zinc nitrate hexahydrate (1.68 g) was dissolved in methanol (80 mL) and 2-methylimidazole (3.70 g) was dissolved in methanol (80 mL). The two solutions were mixed and vigorously stirred for 24 h at room temperature. The resultant particles were collected by centrifugation, washed with methanol (3×), and dried under vacuum overnight at 80 °C.

Synthesis of PCN-224: The synthesis of PCN-224 was based on a modified previous report.[11f] Typically, $ZrCl_4$ (0.15 g), H_2TCPP (0.05 g), and benzoic acid (1.75 g) in DMF (10 mL) were ultrasonically dissolved in a Teflon-lined stainless-steel autoclave (20 mL). The autoclave was sealed and maintained at 120 °C for 24 h. After cooling to room temperature, the solid was collected by filtration, washed with DMF (3×) and acetone (1×), and immersed in acetone for over 12 h. The mixture was centrifuged and dried under vacuum overnight.

Synthesis of porous carbon materials

Synthesis of MOF-5-*T*: Typically, MOF-5 powder (0.50 g) was transferred into a tube furnace. The furnace was heated at 600, 700, 800, 900, and 1000 °C, respectively, with a heating rate of 5 °C min^{-1} in a nitrogen-gas flow (flow rate: ≈60 mL min^{-1}). The furnace was held at this temperature for 1 h and allowed to cool to room temperature to yield a black powder. The obtained powder was washed with an aqueous solution of HCl (3×, except for the powder pyrolyzed at 900 and 1000 °C, in which the generated ZnO was reduced by carbon to give evaporative Zn at such a high temperature)[9a,b] to remove the Zn and/or ZnO species. The black powder was collected by centrifugation, washed with distilled water (3×) and ethanol (3×), and dried under vacuum at 120 °C.

Synthesis of ZIF-8-*T*: Typically, ZIF-8 powder (0.50 g) was transferred into a tube furnace. The furnace was heated at 600, 700, 800, 900, and 1000 °C, respectively, with a heating rate of 5 °C min^{-1} in a nitrogen-gas flow (flow rate: ≈60 mL min^{-1}). The furnace was held at this temperature for 1 h and allowed to cool to room temperature to yield a black powder. The obtained powder was washed with an aqueous solution of HCl (3×, except for the powders pyrolyzed at 900 and 1000 °C, similar to those for MOF-5-T) to remove the Zn and/or ZnO species. The black powder was collected by centrifugation, washed with distilled water (3×) and ethanol (3×), and dried under vacuum at 120 °C.

Synthesis of PCN-224-*T*: Typically, PCN-224 powder (0.30 g) was transferred into a tube furnace. The furnace was heated at 600, 700, 800, 900, and 1000 °C, respectively, with a heating rate of 5 °C min^{-1} in a nitrogen-gas flow (flow rate: ≈60 mL min^{-1}). The furnace was held at this temperature for 1 h and allowed to cool to room temperature to yield a black powder. The obtained powder was stirred in a solution of HF (20%) at 80 °C for 48 h to remove the ZrO_2 species. The black powder was collected by centrifugation, washed with distilled water (3×) and ethanol (3×), and dried under vacuum at 120 °C.

Catalytic activity evaluation

Typically, 4-NP (1.8 mmol L^{-1}, 6.0 mL) and $NaBH_4$ (649.2 mg) were dispersed in H_2O (100 mL) and stirred at 600 rpm at 25 °C. After introducing, the catalyst MOF-5-*T*, ZIF-8-*T*, or PCN-224-*T* (3.0 mg), UV/Vis spectra were obtained to monitor the reaction kinetics in the range $\lambda = 250$–550 nm. For the recycling measurements, three runs of the reaction were taken for PCN-224-700. After the first run, $NaBH_4$ (649.2 mg) and 4-NP (1.8 mmol L^{-1}, 6.0 mL) were directly added to the reaction mixture for the second run and the process was repeated for the third run.

Computational models and methods

Three molecular models of nitrogen-doped graphene (NG) containing pyridinic, pyrrolic, and graphitic nitrogen species were built, which provided the basis to investigate the adsorption and interaction with the 4-NP molecule. DFT calculations were performed at the hybrid DFT B3LYP/6–31G level by using the Gaussian 09 quantum-chemistry program package.[21] The geometry optimization and electronic structure calculations were carried out on these model molecules, from which information about the charge distributions and density of states (DOS) was extracted. The adsorption energies of the 4-NP molecule to the NG systems were computed by subtracting the energies of the optimized adsorption structures with those of the isolated counterparts.

Acknowledgements

This work was supported by the NSFC (Grants 21371162, 51301159, 21521001, and 21473166), the 973 Program (Grants 2014CB931803 and 2014CB848900), the NSF of Anhui Province (Grant 1408085MB23), the Recruitment Program of Global Experts, and the Fundamental Research Funds for the Central Universities (WK2060190026 and WK2090050027).

Keywords: carbon · doping · metal-free catalysts · metal–organic frameworks · porous materials

[1] a) K. Gong, F. Du, Z. Xia, M. Durstock, L. Dai, *Science* **2009**, *323*, 760–764; b) T. Y. Ma, S. Dai, M. Jaroniec, S. Z. Qiao, *Angew. Chem. Int. Ed.* **2014**, *53*, 7281–7285; *Angew. Chem.* **2014**, *126*, 7409–7413; c) W. Qi, D. Su, *ACS Catal.* **2014**, *4*, 3212–3218; d) R. Liu, D. Wu, X. Feng, K. Müllen, *Angew. Chem. Int. Ed.* **2010**, *49*, 2565–2569; *Angew. Chem.* **2010**, *122*, 2619–2623; e) B. Li, Z. Xu, *J. Am. Chem. Soc.* **2009**, *131*, 16380–16382; f) P. Serp, J. L. Figueiredo in *Carbon Materials for Catalysis*, Wiley, Hoboken, **2009**; g) C. Su, K. P. Loh, *Acc. Chem. Res.* **2013**, *46*, 2275–2285; h) X.-K. Kong, C.-L. Chen, Q.-W. Chen, *Chem. Soc. Rev.* **2014**, *43*, 2841–2857; i) B. Xia, Y. Yan, X. Wang, X. W. Lou, *Mater. Horiz.* **2014**, *1*, 379–399; j) S. Navalon, A. Dhakshinamoorthy, M. Alvaro, H. Garcia, *Chem. Rev.* **2014**, *114*, 6179–6212; k) H. Wang, T. Maiyalagan, X. Wang, *ACS Catal.* **2012**, *2*, 781–794.

[2] a) Y. Shao, J. Sui, G. Yin, Y. Gao, *Appl. Catal. B* **2008**, *79*, 89–99; b) W. J. Lee, U. N. Maiti, J. M. Lee, J. Lim, T. H. Han, S. O. Kim, *Chem. Commun.* **2014**, *50*, 6818–6830; c) W. Li, Y. Gao, W. Chen, P. Tang, W. Li, Z. Shi, D. Su, J. Wang, D. Ma, *ACS Catal.* **2014**, *4*, 1261–1266; d) J. Zhang, X. Liu, R. Blume, A. Zhang, R. Schlögl, D. S. Su, *Science* **2008**, *322*, 73–77; e) X.-H. Li, M. Antonietti, *Angew. Chem. Int. Ed.* **2013**, *52*, 4572–4576; *Angew. Chem.* **2013**, *125*, 4670–4674; f) E. Lam, J. H. Chong, E. Majid, Y. Liu, S. Hrapovic, A. C. W. Leung, J. H. T. Luong, *Carbon* **2012**, *50*, 1033–1043.

[3] a) X. Wang, X. Li, L. Zhang, Y. Yoon, P. K. Weber, H. Wang, J. Guo, H. Dai, *Science* **2009**, *324*, 768–771; b) D. Geng, Y. Chen, Y. Chen, Y. Li, R. Li, X. Sun, S. Ye, S. Knights, *Energy Environ. Sci.* **2011**, *4*, 760–764; c) B. Guo, Q. Liu, E. Chen, H. Zhu, L. Fang, J. R. Gong, *Nano Lett.* **2010**, *10*, 4975–4980; d) L.-F. Chen, Z.-H. Huang, H.-W. Liang, Q.-F. Guan, S.-H. Yu, *Adv. Mater.* **2013**, *25*, 4746–4752; e) J. Yang, M. R. Jo, M. Kang, Y. S. Huh, H. Jung, Y.-M. Kang, *Carbon* **2014**, *73*, 106–113.

[4] a) J. R. Long, O. M. Yaghi, *Chem. Soc. Rev.* **2009**, *38*, 1213–1214; b) H.-C. Zhou, J. R. Long, O. M. Yaghi, *Chem. Rev.* **2012**, *112*, 673–674; c) H. Furukawa, K. E. Cordova, M. O'Keeffe, O. M. Yaghi, *Science* **2013**, *341*, 974–986; d) T. R. Cook, Y.-R. Zheng, P. J. Stang, *Chem. Rev.* **2013**, *113*, 734–777; e) H.-C. Zhou, S. Kitagawa, *Chem. Soc. Rev.* **2014**, *43*, 5415–5418.

[5] a) J. Liu, P. K. Thallapally, B. P. McGrail, D. R. Brown, J. Liu, *Chem. Soc. Rev.* **2012**, *41*, 2308–2322; b) M. P. Suh, H. J. Park, T. K. Prasad, D.-W. Lim, *Chem. Rev.* **2012**, *112*, 782–835; c) J.-R. Li, J. Sculley, H.-C. Zhou, *Chem. Rev.* **2012**, *112*, 869–932; d) Y. He, W. Zhou, G. Qian, B. Chen, *Chem. Soc. Rev.* **2014**, *43*, 5657–5678.

[6] a) D. Farrusseng, S. Aguado, C. Pinel, *Angew. Chem. Int. Ed.* **2009**, *48*, 7502–7513; *Angew. Chem.* **2009**, *121*, 7638–7649; b) A. Corma, H. García, F. X. Llabrés i Xamena, *Chem. Rev.* **2010**, *110*, 4606–4655; c) H.-L. Jiang, Q. Xu, *Chem. Commun.* **2011**, *47*, 3351–3370; d) J. Gascon, A. Corma, F. Kapteijn, F. X. Llabrés i Xamena, *ACS Catal.* **2014**, *4*, 361–378; e) T. Zhang, W. Lin, *Chem. Soc. Rev.* **2014**, *43*, 5982–5993; f) D. Wang, R. Huang, W. Liu, D. Sun, Z. Li, *ACS Catal.* **2014**, *4*, 4254–4260.

[7] a) B. Chen, S. Xiang, G. Qian, *Acc. Chem. Res.* **2010**, *43*, 1115–1124; b) Y. Takashima, V. Martinez, S. Furukawa, M. Kondo, S. Shimomura, H. Uehara, M. Nakahama, K. Sugimoto, S. Kitagawa, *Nat. Commun.* **2011**, *2*, 168; c) L. E. Kreno, K. Leong, O. K. Farha, M. Allendorf, R. P. Van Duyne, J. T. Hupp, *Chem. Rev.* **2012**, *112*, 1105–1125; d) Z. Hu, B. J. Deibert, J. Li, *Chem. Soc. Rev.* **2014**, *43*, 5815–5840.

[8] a) Z. Wang, S. M. Cohen, *Chem. Soc. Rev.* **2009**, *38*, 1315–1329; b) J. An, S. J. Geib, N. L. Rosi, *J. Am. Chem. Soc.* **2009**, *131*, 8376–8377; c) H. Kitagawa, *Nat. Chem.* **2009**, *1*, 689–690; d) P. Horcajada, R. Gref, T. Baati, P. K. Allan, G. Maurin, P. Couvreur, G. Férey, R. E. Morris, C. Serre, *Chem. Rev.* **2012**, *112*, 1232–1268.

[9] a) B. Liu, H. Shioyama, T. Akita, Q. Xu, *J. Am. Chem. Soc.* **2008**, *130*, 5390–5391; b) H.-L. Jiang, B. Liu, Y.-Q. Lan, K. Kuratani, T. Akita, H. Shioyama, F. Zong, Q. Xu, *J. Am. Chem. Soc.* **2011**, *133*, 11854–11857; c) M. Hu, J. Reboul, S. Furukawa, N. L. Torad, Q. Ji, P. Srinivasu, K. Ariga, S. Kitagawa, Y. Yamauchi, *J. Am. Chem. Soc.* **2012**, *134*, 2864–2867; d) T. Palaniselvam, B. P. Biswal, R. Banerjee, S. Kurungot, *Chem. Eur. J.* **2013**, *19*, 9335–9342.

[10] a) S. Ma, G. A. Goenaga, A. V. Call, D.-J. Liu, *Chem. Eur. J.* **2011**, *17*, 2063–2067; b) P. Su, H. Xiao, J. Zhao, Y. Yao, Z. Shao, C. Li, Q. Yang, *Chem. Sci.* **2013**, *4*, 2941–2946; c) D. Zhao, J.-L. Shui, L. R. Grabstanowicz, C. Chen, S. M. Commet, T. Xu, J. Lu, D.-J. Liu, *Adv. Mater.* **2014**, *26*, 1093–1097; d) G. Srinivas, V. Krunqleviciute, Z.-X. Guo, T. Yildirim, *Energy Environ. Sci.* **2014**, *7*, 335–342; e) P. Zhang, F. Sun, Z. Xiang, Z. Shen, J. Yun, D. Cao, *Energy Environ. Sci.* **2014**, *7*, 442–450; f) W. Zhang, Z.-Y. Wu, H.-L. Jiang, S.-H. Yu, *J. Am. Chem. Soc.* **2014**, *136*, 14385–14388; g) S. Zhao, H. Yin,

L. Du, L. He, K. Zhao, L. Chang, G. Yin, H. Zhao, S. Liu, Z. Tang, *ACS Nano* **2014**, *8*, 12660 – 12668; h) Y.-Z. Chen, C. Wang, Z.-Y. Wu, sY. Xiong, Q. Xu, S.-H. Yu, H.-L. Jiang, *Adv. Mater.* **2015**, *27*, 5010 – 5016; i) Q. Lin, X. Bu, A. Kong, C. Mao, X. Zhao, F. Bu, P. Feng, *J. Am. Chem. Soc.* **2015**, *137*, 2235 – 2238; j) F. Zheng, Y. Yang, Q. Chen, *Nat. Commun.* **2014**, *5*, 5261; k) W. Xia, A. Mahmood, R. Zou, Q. Xu, *Energy Environ. Sci.* **2015**, *8*, 1837 – 1866.

[11] a) H. Li, M. Eddaoudi, M. O'Keeffe, O. M. Yaghi, *Nature* **1999**, *402*, 276 – 279; b) D. J. Tranchemontagne, J. R. Hunt, O. M. Yaghi, *Tetrahedron* **2008**, *64*, 8553 – 8557; c) K. S. Park, Z. Ni, A. P. Côté, J. Y. Choi, R. Huang, F. J. Uribe-Romo, H. K. Chae, M. O'Keeffe, O. M. Yaghi, *Proc. Natl. Acad. Sci. USA* **2006**, *103*, 10186 – 10191; d) X.-C. Huang, Y.-Y. Lin, J.-P. Zhang, X.-M. Chen, *Angew. Chem. Int. Ed.* **2006**, *45*, 1557 – 1559; *Angew. Chem.* **2006**, *118*, 1587 – 1589; e) S. R. Venna, J. B. Jasinski, M. A. Carreon, *J. Am. Chem. Soc.* **2010**, *132*, 18030 – 18033; f) D. Feng, W.-C. Chung, Z. Wei, Z.-Y. Gu, H.-L. Jiang, Y.-P. Chen, D. J. Darensbourg, H.-C. Zhou, *J. Am. Chem. Soc.* **2013**, *135*, 17105 – 17110.

[12] a) P. Pachfule, B. P. Biswal, R. Banerjee, *Chem. Eur. J.* **2012**, *18*, 11399 – 11408; b) P. Pachfule, V. M. Dhavale, S. Kandambeth, S. Kurungot, R. Banerjee, *Chem. Eur. J.* **2013**, *19*, 749 – 780.

[13] a) P. Hervés, M. Pérez-Lorenzo, L. M. Liz-Marzán, J. Dzubiella, Y. Lu, M. Ballauff, *Chem. Soc. Rev.* **2012**, *41*, 5577 – 5587; b) N. Pradhan, A. Pal, T. Pal, *Colloids Surf. A* **2002**, *196*, 247 – 257; c) S. Panigrahi, S. Basu, S. Praharaj, S. Pande, S. Jana, A. Pal, S. K. Ghosh, T. Pal, *J. Phys. Chem. C* **2007**, *111*, 4596 – 4605; d) S. Wunder, F. Polzer, Y. Lu, Y. Mei, M. Ballauff, *J. Phys. Chem. C* **2010**, *114*, 8814 – 8820; e) R. Fenger, E. Fertitta, H. Kirmse, A. F. Thünemann, K. Rademann, *Phys. Chem. Chem. Phys.* **2012**, *14*, 9343 – 9349; f) P. Veerakumar, M. Velayudham, K.-L. Lu, S. Rajagopal, *Appl. Catal. A* **2012**, *439*, 197 – 205; g) H. Li, J. Liao, Y. Du, T. You, W. Liao, L. Wen, *Chem. Commun.* **2013**, *49*, 1768 – 1770.

[14] a) S. Gazi, R. Ananthakrishnan, *Appl. Catal. B* **2011**, *105*, 317 – 325; b) X.-K. Kong, Z.-Y. Sun, C. Min, C.-L. Chen, Q.-W. Chen, *Energy Environ. Sci.* **2013**, *6*, 3260 – 3266; c) H. K. Sadhanala, J. Khatei, K. K. Nanda, *RSC Adv.* **2014**, *4*, 11481 – 11485; d) X.-K. Kong, Q.-W. Chen, Z.-Y Lun, *J. Mater. Chem. A* **2014**, *2*, 610 – 613; e) L. Gao, R. Li, X. Sui, R. Li, C. Chen, Q. Chen, *Environ. Sci. Technol.* **2014**, *48*, 10191 – 10197.

[15] a) Y. Lu, Y. Mei, M. Drechsler, M. Ballauff, *Angew. Chem. Int. Ed.* **2006**, *45*, 813 – 816; *Angew. Chem.* **2006**, *118*, 827 – 830; b) S. Sarkar, A. K. Sinha, M. Pardhan, M. Basu, Y. Negishi, T. Pal, *J. Phys. Chem. C* **2011**, *115*, 1659 – 1673; c) M. A. Mahmoud, F. Saira, M. A. El-Sayed, *Nano Lett.* **2010**, *10*, 3764 – 3769; d) M. A. Mahmoud, M. A. El-Sayed, *Nano Lett.* **2011**, *11*, 946 – 953.

[16] a) Y. Mei, Y. Lu, F. Polzer, M. Ballauff, *Chem. Mater.* **2007**, *19*, 1062 – 1069; b) Y.-C. Chang, D.-H. Chen, *J. Hazard. Mater.* **2009**, *165*, 664 – 669; c) J. Zeng, Q. Zhang, J. Chen, Y. Xia, *Nano Lett.* **2010**, *10*, 30 – 35; d) N. Sahiner, H. Ozay, O. Ozay, N. Aktas, *Appl. Catal. B* **2010**, *101*, 137 – 143.

[17] a) Z.-S. Wu, S. Yang, Y. Sun, K. Parvez, X. Feng, K. Müllen, *J. Am. Chem. Soc.* **2012**, *134*, 9082 – 9085; b) Y. Lin, X. Cui, C. Yen, C. M. Wai, *J. Phys. Chem. B* **2005**, *109*, 14410 – 14415; c) Y. Wan, H. Wang, Q. Zhao, M. Klingstedt, O. Terasaki, D. Zhao, *J. Am. Chem. Soc.* **2009**, *131*, 4541 – 4550; d) Z. Lei, Y. Xiao, L. Dang, W. You, G. Hu, J. Zhang, *Chem. Mater.* **2007**, *19*, 477 – 484; e) L. Wang, A. Ambrosi, M. Pumera, *Angew. Chem. Int. Ed.* **2013**, *52*, 13818 – 13821; *Angew. Chem.* **2013**, *125*, 14063 – 14066; f) C. H. Choi, S. H. Park, S. I. Woo, *ACS Nano* **2012**, *6*, 7084 – 7091.

[18] a) X. Kong, Q. Chen, Z. Sun, *ChemPhysChem* **2013**, *14*, 514 – 519; b) J. Liang, Y. Jiao, M. Jaroniec, S. Z. Qiao, *Angew. Chem. Int. Ed.* **2012**, *51*, 11496 – 11500; *Angew. Chem.* **2012**, *124*, 11664 – 11668; c) B. Zheng, P. Hermet, L. Henrard, *ACS Nano* **2010**, *4*, 4165 – 4173.

[19] X. Li, Y. Zhu, W. Cai, M. Borysiak, B. Han, D. Chen, R. D. Piner, L. Colombo, R. S. Ruoff, *Nano Lett.* **2009**, *9*, 4359 – 4363.

[20] K. P.-C. Vollhardt, N. E. Schore in *Organic Chemistry*, 5th ed., Freeman & Company, New York, **2006**.

[21] Gaussian 09, Revision D.01, M. J. Frisch, G. W. Trucks, H. B. Schlegel, G. E. Scuseria, M. A. Robb, J. R. Cheeseman, G. Scalmani, V. Barone, B. Mennucci, G. A. Petersson, H. Nakatsuji, M. Caricato, X. Li, H. P. Hratchian, A. F. Izmaylov, J. Bloino, G. Zheng, J. L. Sonnenberg, M. Hada, M. Ehara, K. Toyota, R. Fukuda, J. Hasegawa, M. Ishida, T. Nakajima, Y. Honda, O. Kitao, H. Nakai, T. Vreven, J. A. Montgomery, Jr., J. E. Peralta, F. Ogliaro, M. Bearpark, J. J. Heyd, E. Brothers, K. N. Kudin, V. N. Staroverov, R. Kobayashi, J. Normand, K. Raghavachari, A. Rendell, J. C. Burant, S. S. Iyengar, J. Tomasi, M. Cossi, N. Rega, N. J. Millam, M. Klene, J. E. Knox, J. B. Cross, V. Bakken, C. Adamo, J. Jaramillo, R. Gomperts, R. E. Stratmann, O. Yazyev, A. J. Austin, R. Cammi, C. Pomelli, J. W. Ochterski, R. L. Martin, K. Morokuma, V. G. Zakrzewski, G. A. Voth, P. Salvador, J. J. Dannenberg, S. Dapprich, A. D. Daniels, Ö. Farkas, J. B. Foresman, J. V. Ortiz, J. Cioslowski, D. J. Fox, Gaussian, Inc., Wallingford CT, **2009**.

Received: December 3, 2015
Published online on February 3, 2016